



Heat-treatment induced defect formation in α -Al matrix in Sr-modified eutectic Al–Si alloy



Xiaorui Liu ^{a, b, c, *}, Benoît Beausir ^{b, c}, Yudong Zhang ^{b, c, **}, Weimin Gan ^d, Hui Yuan ^b, Fuxiao Yu ^e, Claude Esling ^{b, c}, Xiang Zhao ^a, Liang Zuo ^{a, f}

^a Key Laboratory for Anisotropy and Texture of Materials (Ministry of Education), Northeastern University, Shenyang, 110819, China

^b Laboratoire d'Étude des Microstructures et de Mécanique des Matériaux (LEM3), CNRS UMR 7239, Université de Lorraine, 57045, Metz, France

^c Laboratory of Excellence on Design of Alloy Metals for low-mAss Structures (DAMAS), Université de Lorraine, 57045, Metz, France

^d German Engineering Materials Science Centre at MLZ, Helmholtz-Zentrum Geesthacht, 85747, Garching, Germany

^e School of Materials Science and Engineering, Northeastern University, Shenyang, 110819, China

^f Taiyuan University of Science and Technology, Taiyuan, 030024, China

ARTICLE INFO

Article history:

Received 28 June 2017

Received in revised form

27 September 2017

Accepted 28 September 2017

Available online 29 September 2017

Keywords:

Al–Si alloy
Sr modification
Heat treatment
Crystal defects
Spheroidization
Recrystallization

ABSTRACT

An intensive formation of crystal defects in the α -Al matrix of an as-cast Sr-modified eutectic Al–Si alloy, induced by heat treatment with rapid heating, has been studied. This phenomenon arises from the fragmentation of the Si crystals and the diffusion of Al atoms into the cracks of the Si crystals. During the rapid heating process, a large temperature gradient is established within an as-cast Al–Si sample. It creates a tensile environment for the irregular-shaped and interconnected Si crystals, as the thermal expansion coefficient of the α -Al is ten times that of the Si. Under the thermal constraints, some Si crystals are broken, where the cracks produce the so-called “capillary force” that attracts the surrounding α -Al matrix to fill in them. As the migration of the Al atoms is substitutional, the Al diffusion creates fluxes of vacancies to the interior of the α -Al matrix; thus, the crack volume is transferred to the α -Al matrix. Due to the homogeneous distribution of the Si crystals and the random presence of the cracks, the α -Al matrix is subjected to a varied migration of vacancies in site, in quantity and in direction. Such diffusion is further perturbed by local migration of Al atoms to accommodate the spheroidization of the Si induced by its shape instability. In this way, a large amount of crystal defects (vacancies and then dislocations) are produced in the α -Al matrix. The produced crystal defects then promote the recovery and even recrystallization of the α -Al matrix, resulting in its refinement. Such a mechanism of defect production is applicable to polycrystalline materials composed of phases with incompatible thermal and mechanical properties.

© 2017 Elsevier B.V. All rights reserved.

1. Introduction

Al–Si alloys are known as a special class of metal matrix composite (MMC) materials with Si phase embedded in α -Al matrix. The thermal and mechanical properties of the constituent phases are very different. Generally, the Si phase is hard and brittle with

limited thermal expansion (Young's modulus $E_{Si} = 170$ GPa; thermal expansion coefficient $\alpha_{Si} = 2.6 \times 10^{-6} \text{ K}^{-1}$), whereas the α -Al phase is soft and ductile with large thermal expansion capacity (Young's modulus $E_{Al} = 70$ GPa; thermal expansion coefficient $\alpha_{Al} = 26.1 \times 10^{-6} \text{ K}^{-1}$). Under an ideal combination of the two phases, *i.e.* fine spherical Si crystals are distributed homogeneously in a fine equiaxed α -Al matrix [1], superior mechanical properties can be achieved. However, as unmodified commercial Al–Si alloys are usually produced by casting in profit of their excellent castability, which leads to the formation of coarse Si crystals over α -Al matrix. As the Si phase is almost non-deformable, the potential mechanical benefits of the composite structure will be lost. So far, the refinement of the microstructural components, especially the hard and brittle Si phase, has been a subject of many investigations

* Corresponding author. Key Laboratory for Anisotropy and Texture of Materials (Ministry of Education), Northeastern University, Shenyang, 110819, China.

** Corresponding author. Laboratoire d'Étude des Microstructures et de Mécanique des Matériaux (LEM3), CNRS UMR 7239, Université de Lorraine, 57045, Metz, France.

E-mail addresses: liuxiaorui311@outlook.com (X. Liu), yudong.zhang@univ-lorraine.fr (Y. Zhang).

[2–10].

By an addition of certain trace elements (like Na or Sr) to the Al–Si melt, the morphology of Si crystals can be modified from coarse plate-like to fine coral-like or bar-like structures [9]. Three-dimensional (3D) microstructural characterization has demonstrated that the Si crystals in the as-cast eutectic Al–Si alloys appear in a form of percolating network in the α -Al matrix [11]. Such interconnected Si structures are unstable when the alloys are exposed to a high temperature [12]. Disintegration and fragmentation happen first at the joints of the branches or the necks of the Si crystals [13–15], and then spheroidization occurs to the fragmented parts, resulting in the formation of elongated or spherical particles [11,15–17]. The spheroidization process that is mainly driven by capillary force [18] or surface tension generated by surface curvature variation (the so-called shape instability [19]) is realized via either surface self-diffusion [20] or Al–Si interdiffusion at Si/Al interface [21]. Thus, a post heat treatment at relatively high temperature (just below eutectic temperature) is effective for the Si spheroidization. To achieve an optimum strength-ductility combination, the refinement of the α -Al matrix is also essential. For a soft metal without allotropic transformation, the refinement can be realized by recovery and recrystallization after the metal is heavily deformed and a sufficient amount of crystal defects is produced [22]. Thus, hot deformation (especially hot extrusion) is widely used to refine the microstructures of Al–Si alloys [23–25].

It should be noted that the Si phase and the α -Al phase have a very large difference in thermal expansion. Thermal constraints can be created if the temperature of the material is not homogeneous. As the Si phase is brittle with almost zero deformation capacity, it may crack under thermal stresses, resulting in fragmentation. Furthermore, the cracks of the Si crystals produce the “capillary force” acting on the surrounding α -Al matrix. Thus, at elevated temperatures, the thermal constraints and the capillary force could be utilized to generate crystal defects (vacancies and dislocations) in the α -Al matrix for recovery and recrystallization. To validate such a hypothesis, a Sr-modified eutectic Al–Si alloy was selected and investigated in the present work. The defect multiplication in the α -Al matrix was examined, and the possible mechanisms were explored.

2. Experimental details

Binary high-purity Al-12.7 wt % Si alloys with an addition of 400 ppm strontium (Sr) were prepared by the crucible slow solidification method. The raw materials used in this work were pure Al (99.996 wt %) and pure monocrystalline Si (99.999 wt %). For the preparation of Sr modified Al-12.7 wt % Si alloys, pure monocrystalline Si was added to the pure Al melt after the Al melt was held at 850 °C for two hours, then the Al-10 wt % Sr master alloy was added to the Al-Si melt when the melt was cooled to 705 °C. Finally, Sr modified Al-12.7 wt % Si alloys were slowly solidified in the 30 mL alumina crucibles. The detailed process of the alloy preparation by melting and casting was described elsewhere [9]. The as-cast ingots were annealed in a salt bath. They were loaded into the salt bath after the bath temperature reached 520 °C, then isothermally held at 520 °C for different time periods (1 h, 4 h and 8 h), followed by air cooling to room temperature.

Samples for scanning electron microscope (SEM) and electron backscattering diffraction (EBSD) analyses were taken from the middle of the as-cast and the heat-treated ingots by wire-electrode cutting. They were mechanically ground, and then polished with an oxide polishing suspension (OP-S) to remove the stress layers formed by mechanical grinding. To visualize the 3D morphologies of the Si crystals, one sample was further electrolytically polished to

partially dissolve the α -Al matrix with a solution of 20% perchloric acid in methanol for 10 s under 25 V at a temperature lower than 10 °C. Microstructural observations were performed at room temperature using a Zeiss Supra 40 field emission gun SEM. The crystallographic orientation measurements were carried out using a JEOL JSM-6500F SEM equipped with an Oxford EBSD camera and the Aztec online acquisition software package (Oxford Instruments). The EBSD diffraction patterns were acquired at the accelerating voltage of 20 kV in a beam-controlled mode with a step size of 0.1 μm . The full differentiation of the α -Al phase and the Si phase was made using the software – Analysis Tools for Orientation Mapping (ATOM) [26]. The disorientation angle distributions and geometrically necessary dislocation (GND) density tensors of the α -Al phase were analyzed using the Channel 5 software package (Oxford Instruments) and the ATOM software, respectively. The spheroidization degree of the eutectic Si crystals (with aspect ratio <2) was evaluated using the ATOM. To obtain statistical information, the EBSD orientation data were acquired from a sample area of about 0.32 mm^2 .

Samples for transmission electron microscope (TEM) analyses were prepared by the “lift-out” method [27] using a Carl ZEISS Auriga 40 Focused Ion Beam (FIB) workstation (Oberkochen, Germany) equipped with an Orsay Physics CORBA ion column, a multi-gas injection system and a Klocke sample manipulator. The thin foils with a thickness of about 2 μm were first cut out of the bulk samples using a gallium (Ga) liquid metal ion source. They were further thinned to about 150 nm under reduced ion beam current at 30 keV, and then milled at 5 keV to remove the amorphized surface layers induced by ion bombardment. The substructural features of the eutectic α -Al and the eutectic Si in the as-cast and the heat-treated states, like dislocation configurations, were examined with a Philips CM200 TEM equipped with a LaB₆ cathode, a Gatan Orius 833 CCD camera, and the automatic orientation analysis software – Euclid’s Phantasies (EP) [28,29]. The automated orientation determination based on Kikuchi line patterns was performed at the accelerating voltage of 200 kV in a beam-controlled mode with a step size of 20 nm. The measured area is about $2 \times 2 \mu\text{m}^2$.

Samples for in-situ neutron diffraction analyses, having a diameter of 5 mm and a height of 7 mm, were taken from the as-cast ingot. The measurements were performed with the neutron diffractometer STRESS-SPEC located at a thermal beam port of FRM-II in Garching, Germany. The Ge (3 1 1) monochromator was selected to produce neutrons with a wavelength of 1.68 Å. The bulk samples were inserted into an austenitic steel crucible and immersed in the neutron beam with a gauge volume of 5 mm in diameter and 5 mm in height, using argon (Ar) as the protective atmosphere to prevent oxidation at elevated temperatures. They were completely melted by heating to 650 °C and isothermally held at this temperature for 5 min, and then cooled at a rate of 30 °C/min. A K type thermocouple (chromel–alumel) was inserted from the top of the crucible to measure the temperature. The neutron diffraction patterns were collected *in-situ* during the cooling from 520 °C to 47 °C with an acquisition time of 10 s for each measurement. The software StressTextureCalculator (STeCa) was used to extract the information of diffraction peak positions. The (1 1 1)_{Si} and the (1 1 1)_{Al} diffraction peaks were observed at the detector position $2\theta = 37^\circ$ with a detector window of 15° .

3. Results and discussion

3.1. Characteristics of as-cast alloy

3.1.1. As-cast microstructure

Fig. 1 presents the eutectic Si phase in the as-cast Sr-modified

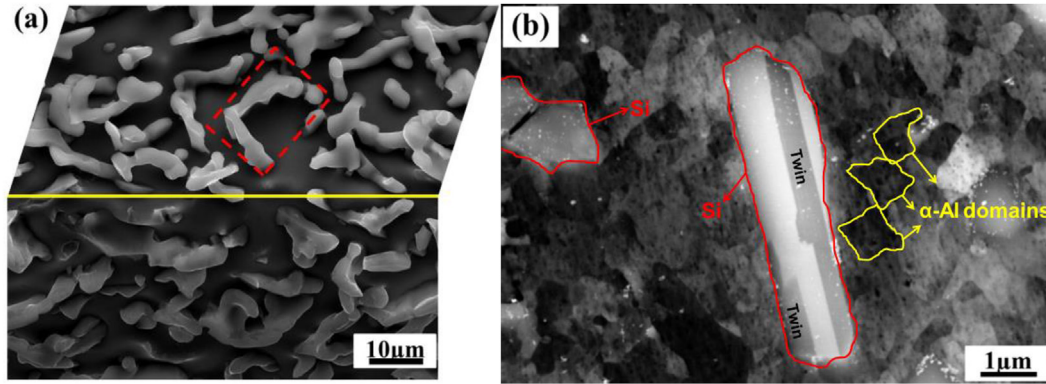


Fig. 1. (a) SEM secondary electron (SE) micrograph displaying 3D morphology of eutectic Si crystals in as-cast Sr-modified Al–12.7Si alloy. The α -Al phase is in dark grey and was partially dissolved, and the Si phase is in light grey. The dashed red rectangle outlines irregular Si segments that are interconnected into coral-like agglomerates. (b) SEM back scattered electron (BSE) micrograph showing twins of Si crystals that are surrounded by contrasted fine α -Al domains. The Si crystals are outline in red and the α -Al domains are indicated in yellow. (For interpretation of the references to colour in this figure legend, the reader is referred to the web version of this article.)

Al–12.7Si alloy, obtained under the SEM secondary electron (SE) imaging mode (Fig. 1a) and the SEM back-scattered electron (BSE) imaging mode (Fig. 1b). Most of the eutectic Si crystals are found to be very irregular in shape. They consist of short bar or narrow plate-shaped segments that are interconnected into coral-like agglomerates, as outlined in the dashed red rectangle in Fig. 1a. The straight parts always contain surface steps and thus their widths and thicknesses are not uniform. Moreover, the eutectic Si crystals, as outlined with red lines in Fig. 1b, are composed of twins with single or multiple orientation variants. Such microstructural features are typical of the eutectic Si in Sr-modified Al–12.7Si alloys. Around the eutectic Si crystals, there are fine α -Al domains (about 1 μm in diameter) with varying contrasts, as outlined with yellow lines as examples in Fig. 1b. As the SEM-BSE contrast of a monophase is determined by its crystallographic orientation, the contrast changes of the α -Al domains suggest that they are crystallographically misoriented. The detailed crystallographic analyses will be given in the later sections.

3.1.2. Thermal lattice strain

Fig. 2 shows the neutron diffraction patterns of the as-cast Sr-modified Al–12.7Si alloy, acquired during the cooling from 520 $^{\circ}\text{C}$ to 47 $^{\circ}\text{C}$ with a rate of 30 $^{\circ}\text{C}/\text{min}$. It can be seen that with the

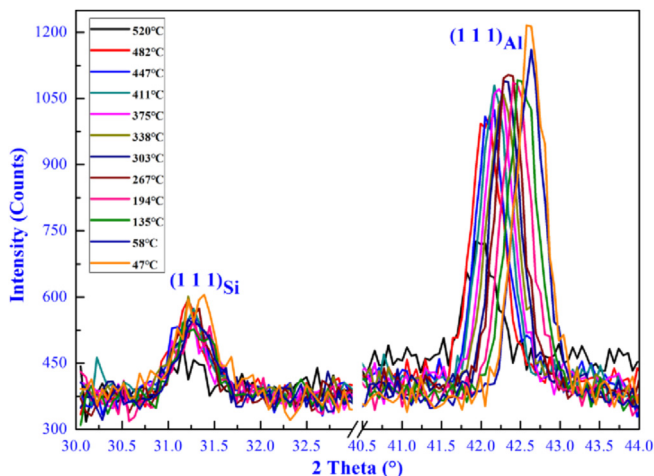


Fig. 2. Neutron diffraction patterns of eutectic Si crystals and α -Al matrix recorded *in situ* during cooling from 520 $^{\circ}\text{C}$ to 47 $^{\circ}\text{C}$ at a cooling rate of 30 $^{\circ}\text{C}/\text{min}$.

decrease of the temperature, the $\{111\}_{\text{Al}}$ peak of the α -Al phase shifts drastically toward the higher 2θ range, whereas the $\{111\}_{\text{Si}}$ peak of the Si phase shifts very slightly. According to the Bragg's law, a significant decrease in the lattice parameters of the α -Al has occurred on cooling. With the determined lattice parameters, the mean lattice strains of the Si phase and the α -Al phase were calculated to be 3×10^{-3} and 13×10^{-3} , respectively. The mean lattice strain of the α -Al phase is about four times that of the Si phase, which corresponds to the difference in thermal expansion coefficient between the two phases. This evidences that the macroscopic thermal expansions of the Si phase and the α -Al phase are achieved by the temperature dependent variations of the lattice constants.

3.2. Microstructural evolution with heat treatment

3.2.1. Eutectic α -Al matrix

Fig. 3 shows the SEM/EBSD band contrast (BC) micrographs of the Sr-modified Al–12.7Si alloy. As the eutectic α -Al colonies are very coarse in millimeter range, only one part of an initial as-cast eutectic colony is presented in each figure. Here, the Si crystals are colored in blue, and the orientation differences within one α -Al colony are outlined in green (from 2 $^{\circ}$ to 4 $^{\circ}$), red (from 4 $^{\circ}$ to 10 $^{\circ}$) and black (higher than 10 $^{\circ}$) lines, respectively. In the as-cast state (Fig. 3a), the α -Al matrix is featured with numerous unclosed boundaries from low angle to high angle and the fine domains enclosed by the low angle boundary segments and the high angle boundary segments. These domains correspond to those revealed by the SEM-BSE contrasts in Fig. 1b. The spatial distributions of the boundaries are relatively homogeneous over the α -Al matrix. After the heat treatment at 520 $^{\circ}\text{C}$ for 1 h (Fig. 3b), some high angle boundaries (>10 $^{\circ}$) started to close up, marking the formation of new “grains” within the α -Al colonies. This indicates that “recrystallization” has occurred during the heat treatment. Unlike the classical recrystallization, no macroscopic deformation was performed to the material before the heat treatment and the newly formed “grains” are not perfect (with disorientation angles up to 4 $^{\circ}$). The number of such “grains” was greatly increased when the isothermal holding time reached 4 h (Fig. 3c), indicating an intensified “recrystallization” of the α -Al matrix. However, after the isothermal holding lasted for 8 h, the number of the “recrystallized” grains was decreased but their sizes were increased, indicating the coarsening of these grains. For some large sized α -Al grains, their grain boundaries were pinned by Si particles. This suggests that the Si particles have a pinning effect on the α -Al boundaries during the

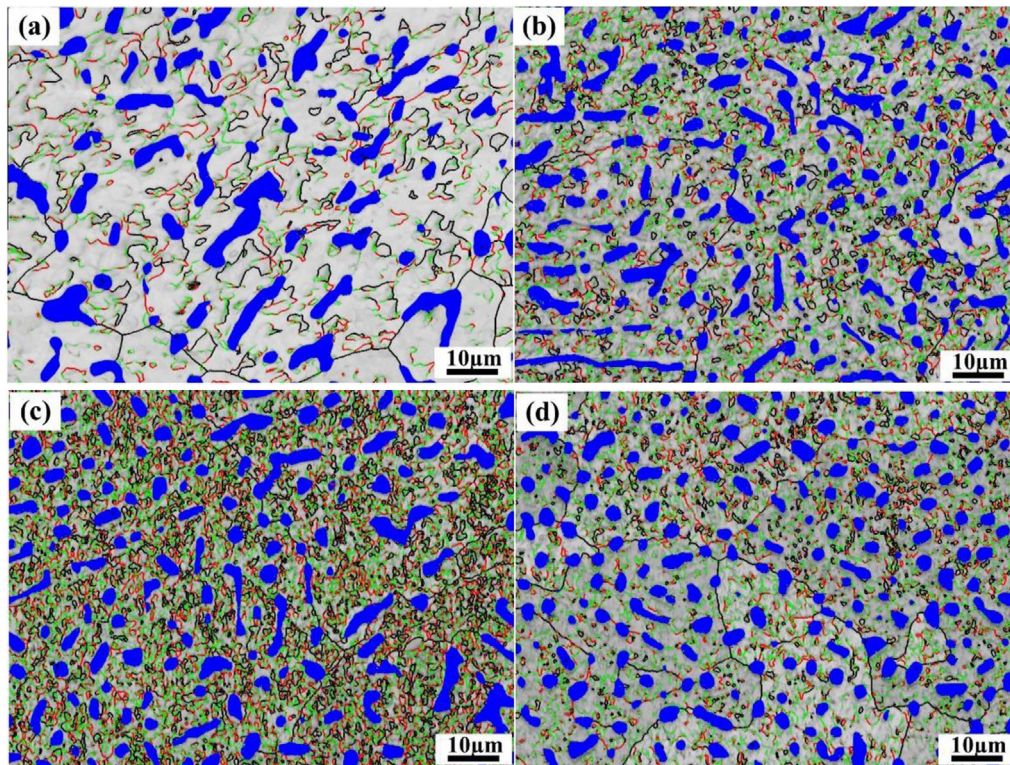


Fig. 3. EBSD band contrast (BC) index micrographs showing microstructural features of eutectic α -Al matrix in Sr-modified Al–12.7Si alloy in (a) as-cast (slowly solidified) state, and after heat treatment at 520 °C for (b) 1 h, (c) 4 h and (d) 8 h. The Si phase is colored in blue. The α -Al boundaries having different disorientation angles are outlined in green (2° – 4°), red (4° – 10°) and black ($>10^\circ$) lines, respectively. (For interpretation of the references to colour in this figure legend, the reader is referred to the web version of this article.)

growth of the “recrystallized” grains through boundary migration (Fig. 3d). Moreover, the formation of the new “grains” was found to occur throughout the α -Al matrix but not preferentially along the Si/Al interphase boundaries where the misfit strains are the highest.

To quantify the “recrystallization” process with the heat treatment time, the area fractions of the “recrystallized” grains were analyzed using the ATOM software, and the results are presented in Fig. 4. The “recrystallized” grains were detected by the flood-fill method [13] with a tolerance angle of 4° . Compared with the as-cast state, the area fraction of the “recrystallized” α -Al matrix

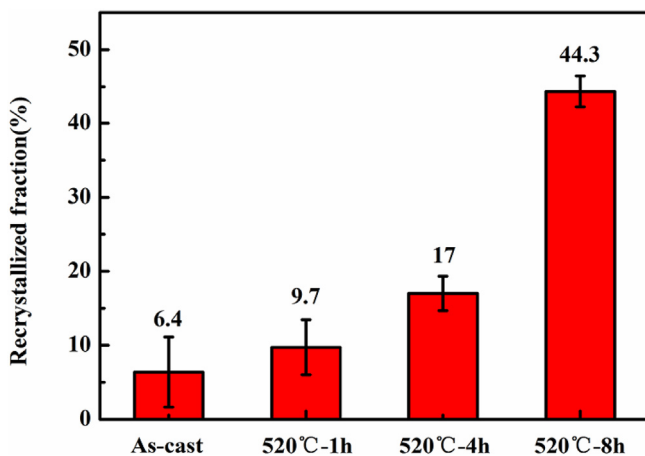


Fig. 4. Variation of area fraction of “recrystallized” α -Al matrix with heat treatment time for Sr-modified Al–12.7Si alloy.

increased with the prolongation of the isothermal holding time, although the alloy did not undergo any macroscopic deformation. In contrast to the usual process of recrystallization, the amount of low angle disorientation ($<4^\circ$) in the newly formed α -Al grains is not reduced but rather increased by this kind of “recrystallization”. Fig. 5 presents the EBSD local disorientation micrographs corresponding to Fig. 3. According to the color scale (blue to red: 0° – 4°) shown in the figure, the quantity of the disoriented zones with a disorientation angle of about 2° in the α -Al matrix was increased from the as-cast state (Fig. 5a) to the heat-treated state with the isothermal holding time of 1 h (Fig. 5b). It reached the maximum after the 4 h isothermal holding (Fig. 5c) and then decreased after the 8 h isothermal holding (Fig. 5d). Note that the disoriented zones are distributed relatively homogeneously within the α -Al matrix without spatial preference with respect to the locations of the Si crystals. They appear even in the regions enclosed by high angle boundaries ($>10^\circ$) that are formed during the heat treatment.

Further TEM observation showed that there are a large number of dislocation arrays and dislocation networks in the α -Al matrix after the heat treatments, as displayed in the TEM bright field (BF) micrographs in Fig. 6a and b. The appearances of dislocation arrays and dislocation networks during the heat treatment indicate that the polygonalization has occurred in the α -Al matrix that is a necessary process for recrystallization. From the grain reference orientation deviation (GROD) [30] micrograph (Fig. 6c), it is seen that some sub-grains with low angle boundaries were formed. This confirms that the formation of the “recrystallized” grains revealed by the EBSD misorientation micrographs in Fig. 5b and c is realized by dislocation rearrangements, as in the case of classic recrystallization of deformed metals. However, apart from the dislocation arrays and dislocation networks, numerous discrete or individual dislocations in the α -Al matrix appear, as shown in Fig. 6d. Such

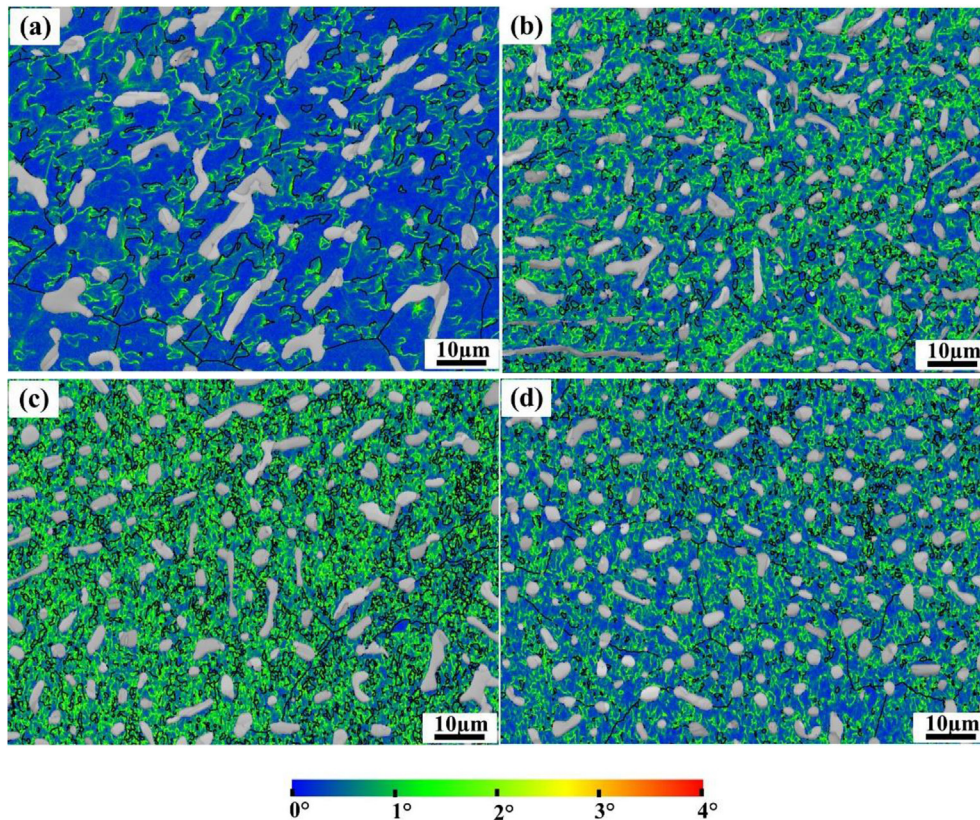


Fig. 5. Local disorientation micrographs of eutectic α -Al matrix in Sr-modified Al–12.7Si alloy, obtained (a) in as-cast (slowly solidified) state and after heat treatment at 520 °C for (b) 1 h, (c) 4 h and (d) 8 h. The Si phase is colored in gray, and the high angle boundaries ($>10^\circ$) in α -Al matrix are marked with black lines.

dislocations should account for the local disorientations within the “recrystallized” grains, as revealed in Fig. 5b and c. The two kinds of characteristic dislocation configurations (array/network and individual) suggest that two opposite processes occurred during the heat treatments. One is the dislocation rearrangement that leads to the recovery and recrystallization of the α -Al matrix and the reduction of the number of dislocations, and the other is the generation of dislocations that multiplies the number of dislocations. As for the eutectic Si crystals, almost no dislocations were observed.

To evaluate the heat-treatment induced dislocation density change in a statistical sense, the planar GND density tensors of the as-cast and the heat-treated samples were calculated using the measured EBSD orientation data. In the calculations, we only took into account the pixels with the correlated disorientation angles within the range from 1° to 4° , considering that the disorientation angles below 1° may be caused by the angular imprecision of the SEM/EBSD measurement system and those higher than 4° correspond to sub-grain boundaries. The results are presented in terms of the average entrywise norms of the GND density tensor in Fig. 7. It is seen that the density of GND in the α -Al matrix increases from the as-cast state to the heat-treated states, reaching the maximum after the heat treatment for 4 h.

3.2.2. Eutectic Si crystals

Fig. 3 demonstrates that the initially interconnected and branched eutectic Si crystals become fragmented and spheroidized during the heat treatments, alongside with the dislocation multiplication of the eutectic α -Al matrix. In consequence, the number of the Si particles increases with the increased isothermal holding time. Due to the fragmentation and the spheroidization, the morphologies of the Si crystals evolve from the curved bar

shape in the as-cast state (Fig. 3a) to the short straight bar shape after the isothermal holding of 1 h (Fig. 3b) and of 4 h (Fig. 3c) and finally to nearly spherical shape after the isothermal holding of 8 h (Fig. 3d). To assess such morphological evolutions, the quantities of the eutectic Si crystals with different aspect ratios were analyzed and the results are displayed in Fig. 8. It is seen that with the increase of the isothermal holding time, the amount of the Si crystals having small aspect ratios (<2 , representing nearly equiaxed shape) increases, whereas that with large aspect ratios (>4) decreases, indicating the fragmentation of the large sized eutectic Si crystals. The small difference between Fig. 8b and c indicates that the fragmentation happened mainly during the first 4 h of isothermal holding, whereas only the spheroidization happened to the fragmented Si particles during the subsequent 4 h of isothermal holding. This result suggests that the fragmentation process of the Si crystals was concomitant to the process of the formation of the dislocations in the α -Al matrix, *i.e.* the two processes are interrelated.

A close examination on the 3D morphologies of the Si crystals in the as-cast and heat-treated states has allowed revealing the characteristics of the eutectic Si fragmentation, as shown in Fig. 9. The morphological evolution of the Si crystals with the heat treatment time underwent three steps. First, the disconnection of the eutectic Si crystals happened at the joints of the interconnected bars, as seen in Fig. 9a (520 °C–1 h). Then, it occurred at the “necks” of the straight bars where the thickness or width changes, as shown in Fig. 9b (520 °C–4 h), 9c and 9d (520 °C–8 h). Finally, the fragmented Si crystals became spheroidal and enveloped with flat facets, as displayed in Fig. 9e (520 °C–8h). By a detailed characterization, it is confirmed that the facets are mostly the $\{111\}_{\text{Si}}$ planes, *i.e.* the close packed planes having the lowest surface energy for a

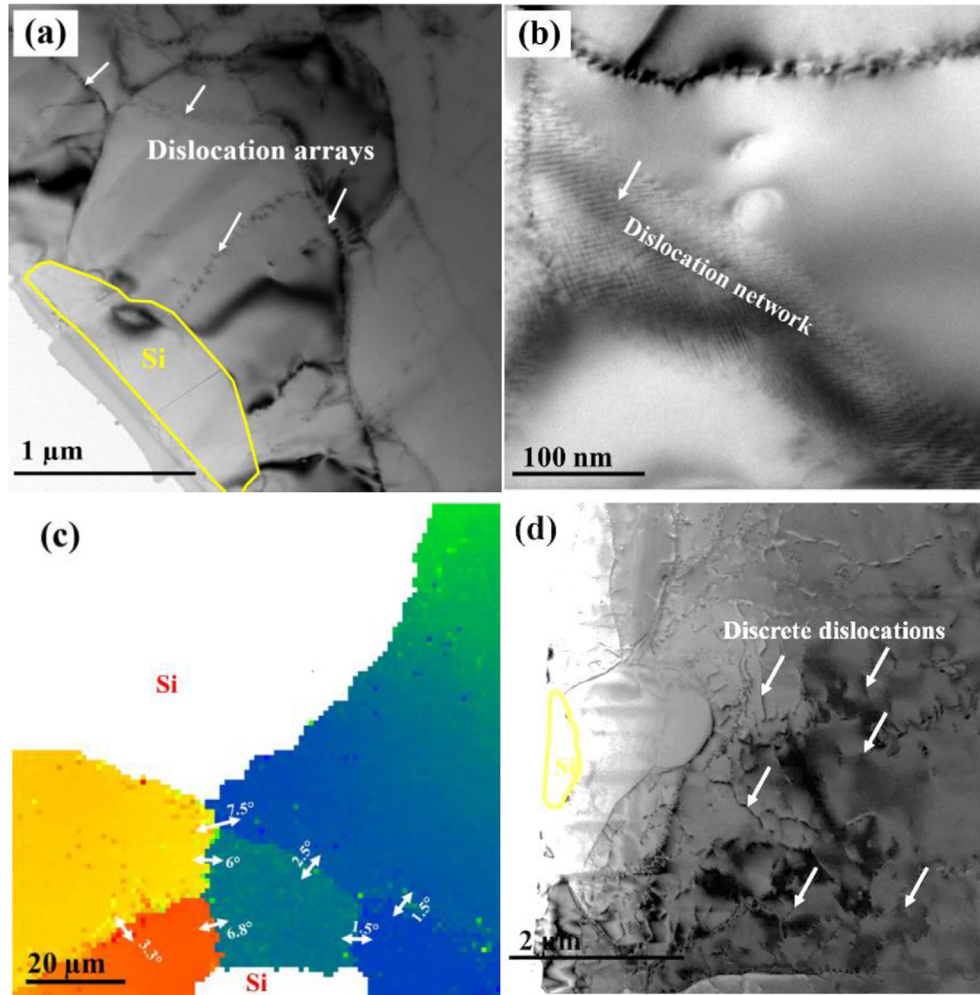


Fig. 6. TEM bright field micrographs presenting (a) dislocation arrays and (b) dislocation networks in α -Al matrix after heat treatment at 520 °C for 4 h (c) GROD micrograph (from TEM orientation micrograph) illustrating sub-grains with low angle boundaries formed through polygonalization. (d) TEM bright field micrograph showing individual dislocations in α -Al matrix.

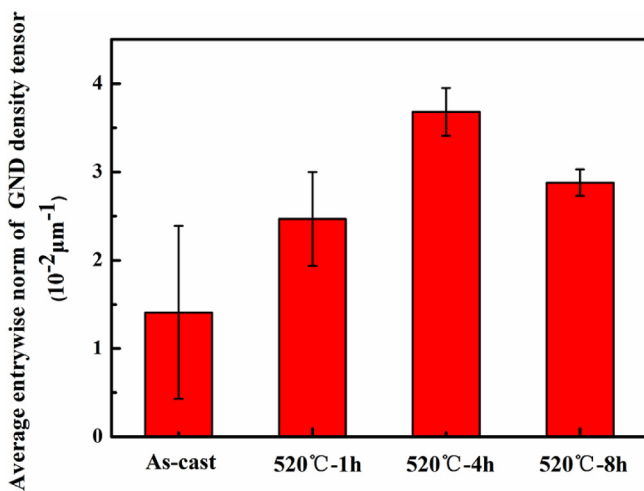


Fig. 7. Calculated entrywise norms of GND density tensor of α -Al matrix in as-cast and heat-treated states. The maximum allowed disorientation angle is 4°.

diamond structured Si crystal [31,32]. The two kinds of ruptures, namely the ductile rupture with obvious necking (Fig. 9b) and the

brittle rupture with flat rupture surface (Fig. 9c and d), indirectly evidence the occurrence of two micro-processes for the Si fragmentation. One is the surface self-diffusion [20] or Al–Si interdiffusion at Si/Al interfaces [21] under the surface tension generated by Si surface curvature variation, and the other the cleavage fracture induced by local mechanical constraints. Further examination revealed that the cleavage plane is the $\{111\}_{\text{Si}}$ and in the most cases the cleavage is initiated on the $\{111\}_{\text{Si}}$ twinning planes, as shown in Fig. 10a as an example. It is worth mentioning that during the fragmentation and the spheroidization, the fragmented Si crystals tend to be spatially separated, accompanied by a rotation of less than 15°, as shown in Fig. 10b. After the heat treatments, no voids or cracks were visible between the separated parts of the Si crystals. All cracks were eventually filled by α -Al.

4. Discussion

When a solid sample is subjected to heating, heat is transferred from its surface to its interior. A long range positive temperature gradient ($\Delta T > 0$) can be created between the hot end (exterior) and the cold end (interior) of the sample. This results in a positive expansion gradient ($\Delta a > 0$) in the direction from the sample interior to the sample surface, as illustrated in Fig. 11a. The magnitude of the temperature gradient and its spatial spread are heating rate

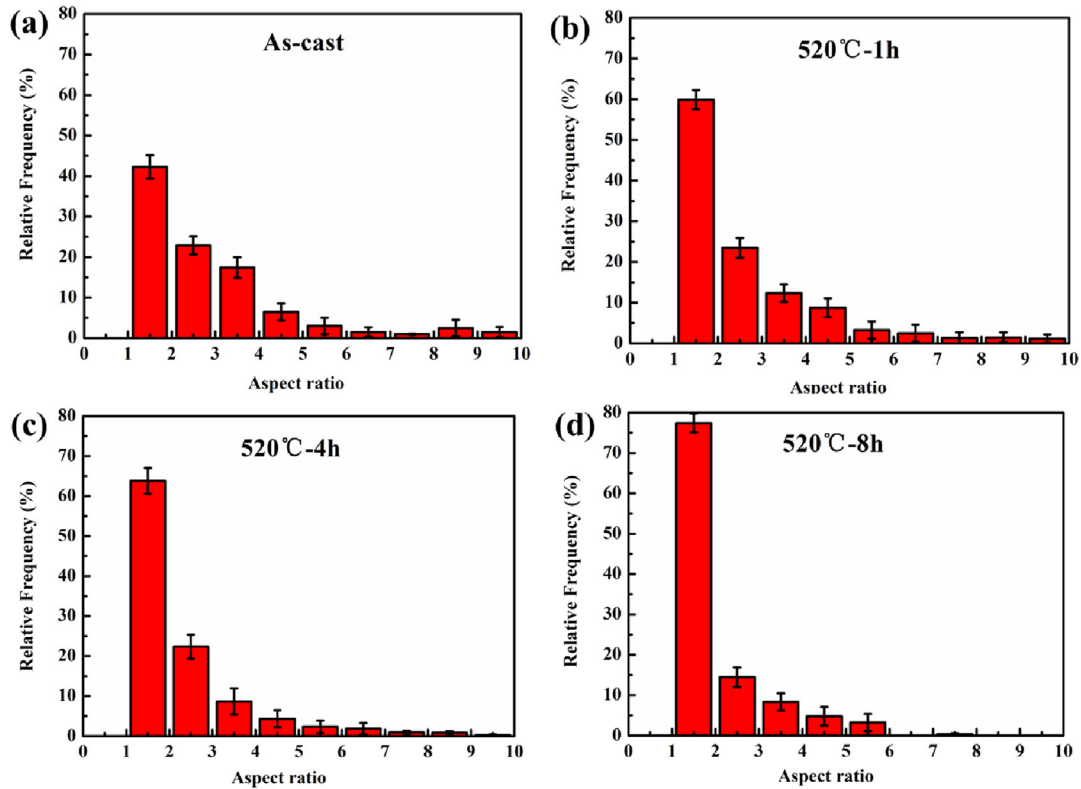


Fig. 8. Relative frequencies of eutectic Si crystals with different aspect ratios in as-cast and heat-treated Sr-modified Al–12.7Si alloys.

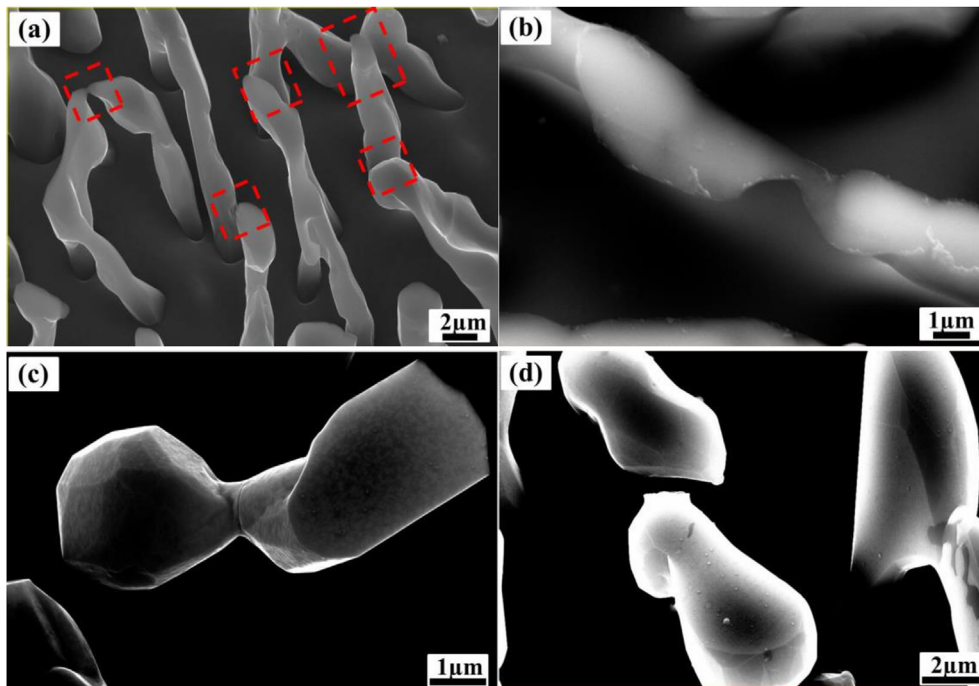


Fig. 9. SEM SE images showing disconnection, fragmentation, and spheroidization of eutectic Si crystals in Sr-modified Al–12.7Si alloy after heat treatment: (a) 520 °C-1 h, disconnection at joints (outlined with dashed red rectangles); (b) 520 °C-4 h, necking at a straight bar; (c), (d) and (e) 520 °C-8 h, crack nucleation, cleavage fracture and spheroidization of Si crystals. (For interpretation of the references to colour in this figure legend, the reader is referred to the web version of this article.)

dependent, *i.e.* the higher the heating rate, the higher the magnitude and the shorter the spatial spread. Under the temperature gradient, tension is produced along the expansion gradient, as

schematically illustrated in Fig. 11a. At the isothermal holding stage, a homogeneous temperature field is established throughout the sample if the holding time is long enough. The mechanical

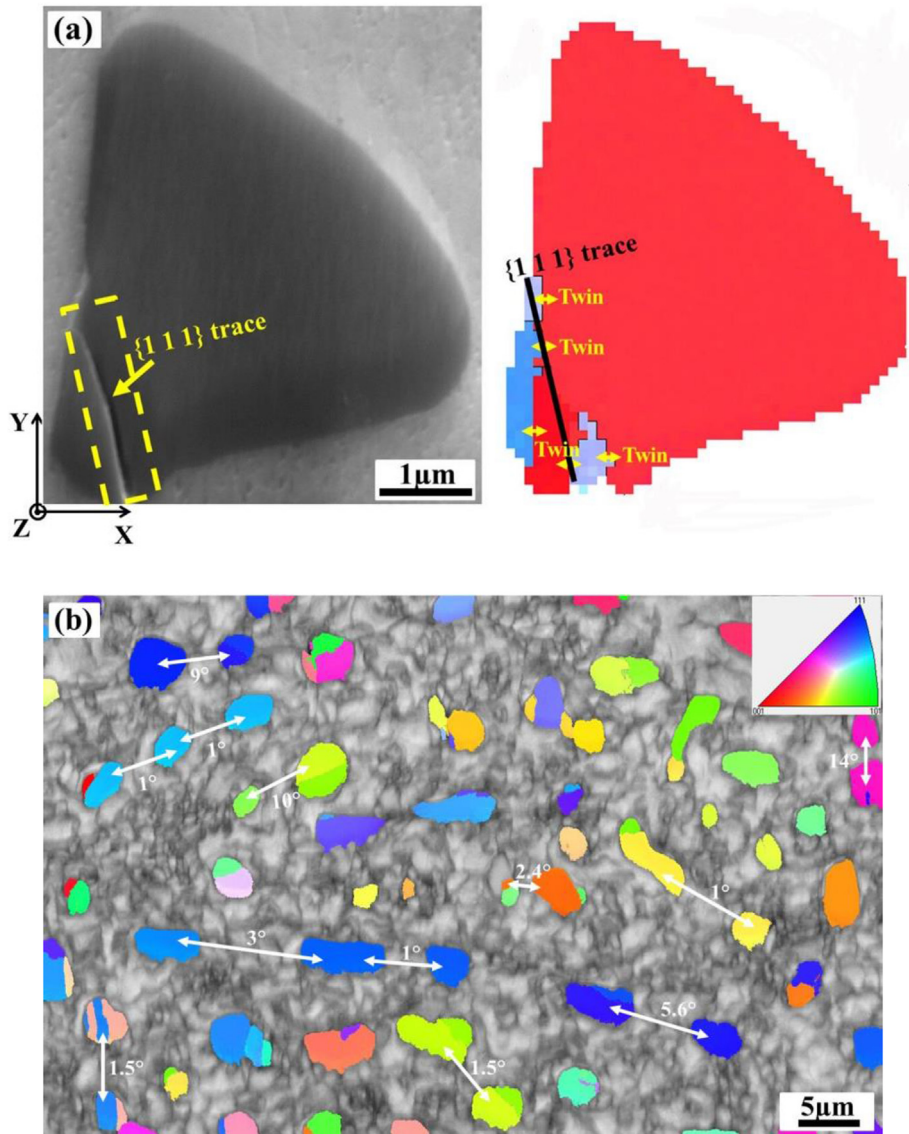


Fig. 10. (a) SEM SE micrograph (left) and EBSD orientation micrograph (right) showing cleavage initiated on $\{1\ 1\ 1\}_{\text{Si}}$ twinning plane of eutectic Si in Sr-modified Al–12.7Si alloy (heat treated at 520 °C for 4 h). The crack site is outlined with dashed yellow rectangle and the trace of the $\{1\ 1\ 1\}$ plane is marked with black line. The α -Al matrix is colored in white. (b) EBSD micrograph showing fragmented and separated Si crystals. The Si crystals are colored according to their orientations as indicated in the inset (Y-axis inverse pole figure), where the α -Al matrix is represented with band contrast. (For interpretation of the references to colour in this figure legend, the reader is referred to the web version of this article.)

constraints due to the long range temperature variation disappear. When the sample is cooled, the heat is transferred from its interior to its surface. A negative temperature gradient ($\Delta T < 0$) is established from the sample surface to the sample interior with respect to that of the heating process, creating a contraction gradient ($\Delta\alpha < 0$), as illustrated in Fig. 11b. Obviously, the heating mode applied in the present heat treatment (*i.e.* the direct dipping of the samples in the 520 °C salt bath) should generate larger temperature gradients and expansion gradients in the treated samples in the heating process than in the cooling process.

For the present alloy, the α -Al phase is of majority in terms of the volume fraction, and the Si phase is in smaller size and it is distributed homogeneously in the α -Al matrix (Fig. 1). The thermal expansion or contraction amount of the material is thus mainly defined by the α -Al matrix. As the thermal expansion coefficient of the α -Al is about 4 times that of the Si, the thermal expansions or contractions of the two phases are largely incompatible. Thus, mechanical constraints are inevitably created between the two

phases. For the Si crystals, only about 1/4 of the thermal expansion or contraction created by the α -Al can be assimilated through their own thermal expansion or contraction. The rest needs to be accommodated either by the deformation of the surrounding α -Al matrix as it is soft or by cracking of the Si crystals as they are brittle.

By the application of the rapid heating in the present heat treatments, a tensile environment was established from the sample surface to the sample interior (Fig. 11a). Since the as-cast eutectic Si crystals were irregularly shaped and interconnected into coral-like agglomerates with sharp turns and surface steps, they became more fragile to the tensile thermal stresses (Fig. 11a). Thus, cracking occurred easily at the joints of the branches or the necks of the Si crystals. To accommodate the thermal expansion of the surrounding α -Al matrix, the fractured parts were pulled away and the crack volumes were enlarged. Due to the shape irregularity of the Si crystals, the mechanical constraints (mainly tension along the expansion gradient) were locally deviated in direction and in magnitude. Thus, accompanying the enlargement of the cracks, the

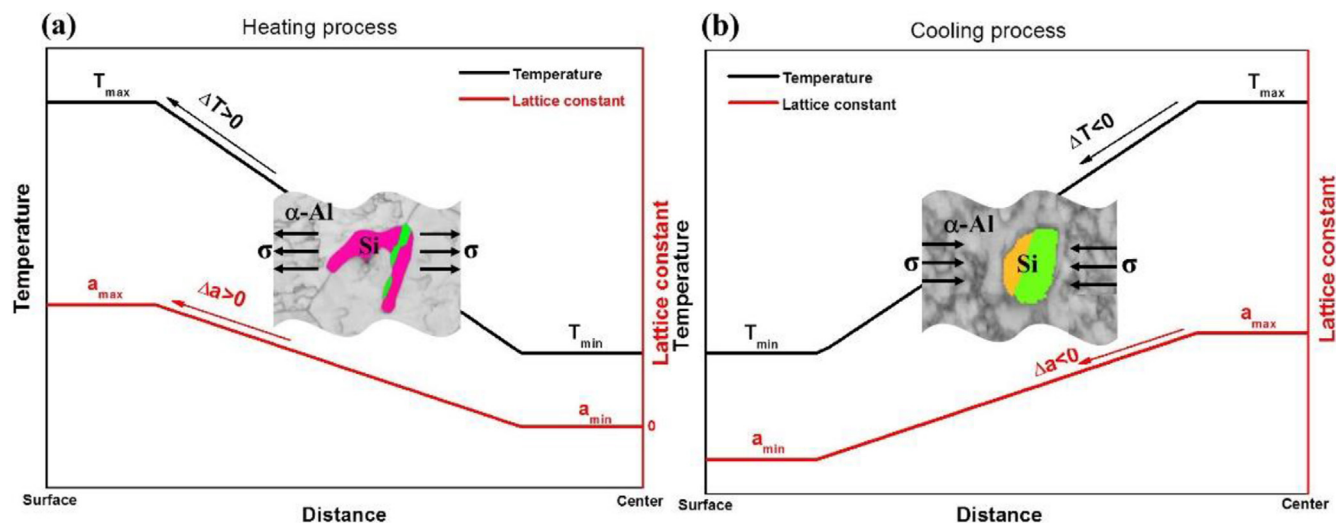


Fig. 11. Illustration of variations of temperature and lattice constant from sample surface to sample interior during (a) heating process and (b) cooling process. For simplicity, linear variations are assumed.

fragmented parts also rotated, leading to the orientation changes of these parts, as shown in Fig. 9. As the temperature gradient swept the whole sample volume before the set temperature was reached, all the Si crystals had a chance to undergo certain mechanical constraints and thus to crack (partially or totally).

During the isothermal holding, the mesoscopic mechanical constraints induced by the thermal expansion incompatibility between the two phases disappeared. However, nanoscaled and even atomic-scaled mechanical constraints can exist, like the capillary force induced by cracks and the surface tension induced by curvature variations of the Si crystals. These mechanical constraints provoked atomic diffusion in the α -Al matrix around the cracks of the Si crystals, as the material was exposed to a relatively high temperature (520 °C that is 57 °C below the melting point). Under the induced capillary force, the Al atoms diffused substitutionally toward the crack regions, creating fluxes of vacancies in the opposite directions. In such a way, the crack volumes between the fractured Si crystals were fully filled with the Al atoms, and the generated vacancies were progressively transformed into clusters and transferred to the interiors of the α -Al matrix. Fig. 12 illustrates the fragmentation process and the spheroidization process of the Si crystals, accompanied by the substitutional diffusion in the surrounding α -Al matrix. As shown in Fig. 12a, each α -Al zone delimited by the fractured Si crystals (as circled in the figure) is subjected to the migration of Al atoms to the crack regions of those Si crystals having different orientations, shapes and sizes. Thus, the substitutional diffusion happened in various directions with different vacancy fluxes. As a result, the vacancy concentration gradients were created in the volume and they eventually evolved into dislocations, making the α -Al crystals defective. Together with the local diffusion of the Al atoms that was required to accommodate the Si diffusion (arrowed in black in Fig. 12b) induced by the shape instability of the Si crystals [33], the defective regions were further enlarged and spreaded over the α -Al matrix with a prolonged isothermal holding time.

When the cooling began, the thermal contraction amount was also dominated by the α -Al phase, similarly to the heating process. In such a circumstance, the Si crystals were subjected to a compression by the surrounding α -Al matrix. Clearly, a large portion of the thermal contraction of the α -Al matrix could not be accommodated by the Si crystals. As the Si phase is much harder under compression, the thermal contraction has to be

accommodated by the α -Al phase through plastic deformation, giving rise to the formation of the crystal defects (dislocations) in the α -Al matrix. However, for the present heat treatments, the heating rate was much higher (the cold samples were dipped very rapidly in the salt bath of 520 °C) than the cooling rate (air cooling). The temperature gradient on heating should be much larger in magnitude and much narrower in distance than those on cooling. Thus, the mechanical constraints during the heating were much more intense and the thermal stresses acting on the Si crystals and on the α -Al matrix were much higher. Moreover, the shape irregularity and the interconnecting feature of the as-cast eutectic Si crystals further aggravated the destructive effect of the thermal stresses. In this connection, the formation of cracks in the Si crystals and the crystal defects in the α -Al matrix should be dominant during the heating and the subsequent isothermal holding.

Once the crystal defects (vacancies and dislocations) were created, the stored energy of the material was increased. Then, recovery and recrystallization happened at the elevated temperature (during isothermal holding), leading to the formation of the fine α -Al domains with low angle or high angle boundaries. Two processes, *i.e.* defect formation and defect annihilation, progressed dynamically and in competition during the isothermal holding. At the early stage, the filling of α -Al atoms into the cracks of the fractured Si crystals and the Si diffusion induced by shape instability were prevalent. Thus, the defect multiplication was dominant, as evidenced by the increased amount of local disorientations (around 2°) in Fig. 5a to c and further confirmed by a large number of individual dislocations in Fig. 6d. With the prolongation of the isothermal holding time, the cracks of the Si crystals were mostly filled, and the number of Si particles was increased but their aspect ratios were decreased. As the microscopic diffusion became less intensive, the recovery and recrystallization prevailed over the defect multiplication. The dislocations in the “recrystallized” grains formed in the α -Al matrix became less and the “recrystallized” grains started to grow (Fig. 5d). Due to the continuous and irregular movements of Al atoms in the α -Al matrix induced by defect formation and by recovery and recrystallization, the fractured Si particles moved and rotated with the surrounding α -Al matrix. Thus, the spatial distances and orientation differences between the fractured Si particles were further enhanced, making them more randomly oriented.

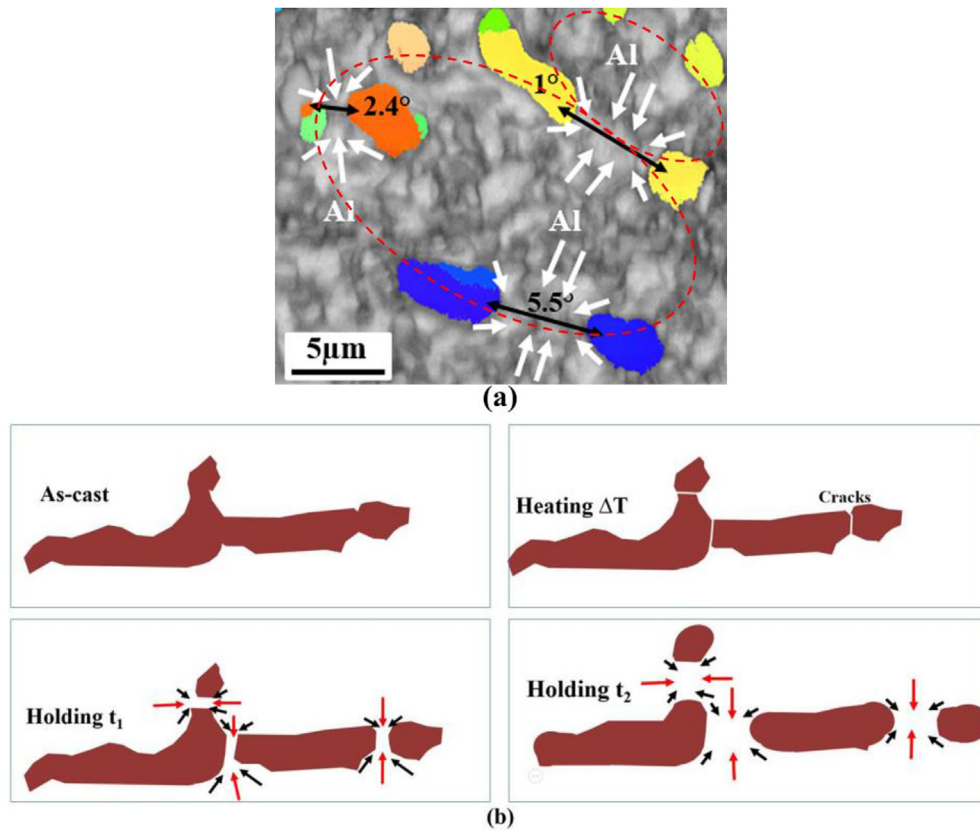


Fig. 12. Illustrations of fragmentation and spheroidization of Si crystals and substitutional diffusion in adjacent α -Al matrix. In (a), α -Al zones delimited by Si crystals are circled with red line, and fragmented Si crystals are indicated with double-headed black arrows. The white arrows indicate the diffusion of Al atoms. In (b), two diffusion processes of Al atoms - induced by cracks of Si crystals and by Si spheroidization - are indicated with the single-headed red and black arrows, respectively. (For interpretation of the references to colour in this figure legend, the reader is referred to the web version of this article.)

5. Summary

In the present study, a eutectic Al–12.7Si alloy with a 400 ppm Sr addition was slowly cast, and then directly annealed at 520 °C for different time periods (1 h, 4 h and 8 h). It was demonstrated that the microstructural evolutions during the heat treatments involve intensive formation of crystal defects in the α -Al matrix with no macroscopic deformation. This unique character should be mainly attributed to the fragmentation and spheroidization of the eutectic Si crystals that are coral-like shaped with sharp corners and surface ridges or edges in the as-cast state. When the as-cast sample is subjected to the rapid heating, a large temperature gradient is created and it sweeps through the whole sample volume from the surface to the center. Due to the limited accommodating capacity of the Si crystals to the large thermal expansion of the surrounding α -Al matrix, the as-cast eutectic Si crystals tend to crack at their fragile places, like sharp corners for example. During the isothermal holding, the Al atoms are attracted to fill the cracks of the Si crystals under the capillary force created by these cracks, which generates fluxes of vacancies in the opposite directions. Since the fractured Si crystals are distributed homogeneously in the α -Al matrix, the spatial diffusion of the vacancies can proceed in various directions. Moreover, such a defect transfer is perturbed by the local diffusion of Al atoms to accommodate the shape change of the Si crystals during spheroidization. In consequence, the α -Al matrix is severely deformed. As the defect multiplication happens at the high temperature, recovery and even recrystallization occurs, leading to the refinement of the α -Al matrix.

The defect multiplication mechanism revealed in the present

work is applicable to other materials composed of two phases with large thermal expansion difference and large Young's modulus difference, such as composite materials. In this context, the present results provide useful information for designing heat treatment process to achieve optimal strength-ductility combination through integrating the spheroidization of the hard phase and the refinement of the ductile matrix phase.

Acknowledgements

This work is supported by the 111 Program of China (Grant No. B07015) and the Program for Liaoning Innovative Research Team in University (Grant No.LT2013007). X.R. Liu is grateful to the China Scholarship Council for providing the PhD Scholarship (Grant No. 201306080056).

References

- [1] J.F. Su, X. Nie, V. Stoilov, Characterization of fracture and debonding of Si particles in AlSi alloys, *Mater. Sci. Eng. A* 527 (2010) 7168–7175.
- [2] C.L. Xu, Q.C. Jiang, Y.F. Yang, H.Y. Wang, J.G. Wang, Effect of Nd on primary silicon and eutectic silicon in hypereutectic Al–Si alloy, *J. Alloys Compd.* 422 (2006) L1–L4.
- [3] F.C. Robles Hernández, J.H. Sokolowski, Comparison among chemical and electromagnetic stirring and vibration melt treatments for Al–Si hypereutectic alloys, *J. Alloys Compd.* 426 (2006) 205–212.
- [4] W. Prukkanon, N. Srisukhumbowornchai, C. Limmaneevichitr, Modification of hypoeutectic Al–Si alloys with scandium, *J. Alloys Compd.* 477 (2009) 454–460.
- [5] A.K. Prasada Rao, M. Mahfoud, Effect of cadmium on the microstructure of Al–7Si alloy, *J. Alloys Compd.* 491 (2010) L8–L10.
- [6] U. Patakham, J. Kajornchaiyakul, C. Limmaneevichitr, Modification mechanism

- of eutectic silicon in Al-6Si-0.3Mg alloy with scandium, *J. Alloys Compd.* 575 (2013) 273–284.
- [7] S. Farahany, A.K. Dahle, A. Ourdjini, A. Hekmat-Ardakan, Flake-fibrous transition of silicon in near-eutectic Al-11.7Si-1.8Cu-0.8Zn-0.6Fe-0.3Mg alloy treated with combined effect of bismuth and strontium, *J. Alloys Compd.* 656 (2016) 944–956.
- [8] M. Timpel, N. Wanderka, B.S. Murty, J. Banhart, Three-dimensional visualization of the microstructure development of Sr-modified Al-15Si casting alloy using FIB-EsB tomography, *Acta Mater.* 58 (2010) 6600–6608.
- [9] X.R. Liu, Y.D. Zhang, B. Beausir, F. Liu, C. Esling, F.X. Yu, X. Zhao, L. Zuo, Twin-controlled growth of eutectic Si in unmodified and Sr-modified Al-12.7%Si alloys investigated by SEM/EBSD, *Acta Mater.* 97 (2015) 338–347.
- [10] J.H. Li, X.D. Wang, T.H. Ludwig, Y. Tsunekawa, L. Arnberg, J.Z. Jiang, P. Schumacher, Modification of eutectic Si in Al-Si alloys with Eu addition, *Acta Mater.* 84 (2015) 153–163.
- [11] F. Lasagni, A. Lasagni, E. Marks, C. Holzappel, F. Mücklich, H.P. Degischer, Three-dimensional characterization of 'as-cast' and solution-treated AlSi12(Sr) alloys by high-resolution FIB tomography, *Acta Mater.* 55 (2007) 3875–3882.
- [12] S. Joseph, S. Kumar, V.S. Bhadram, C. Narayana, Stress states in individual Si particles of a cast Al-Si alloy: micro-Raman analysis and microstructure based modeling, *J. Alloys Compd.* 625 (2015) 296–308.
- [13] P.Y. Zhu, Q.Y. Liu, T.X. Hou, Spheroidization of eutectic silicon in Al-Si alloys, *Trans. Am. Foundrymen's Soc.* 93 (1985) 609–614.
- [14] E. Ogris, Development of Al-Si-Mg Alloys for Semi-Solid Processing and Silicon Spheroidization Treatment (SST) for Al-Si cast alloys, Institute of Metallurgy, ETH Zürich, 2002. Ph.D Thesis.
- [15] R.Y. Wang, W.H. Lu, Spheroidization of eutectic silicon in direct-electrolytic Al-Si alloy, *Metall. Mater. Trans. A* 44 (2013) 2799–2809.
- [16] G. Requena, G. Garcés, M. Rodríguez, T. Pirling, P. Cloetens, 3D architecture and load partition in eutectic Al-Si alloys, *Adv. Eng. Mater.* 11 (2009) 1007–1014.
- [17] E. Ogris, A. Wahlen, H. Lüchinger, P.J. Uggowitzer, On the silicon spheroidization in Al-Si alloys, *J. Light Met.* 2 (2002) 263–269.
- [18] J.C.M. Kampe, T.H. Courtney, Y. Leng, Shape instabilities of plate-like structures — I. Experimental observations in heavily cold worked in situ composites, *Acta Metall.* 37 (1989) 1735–1745.
- [19] G. Sharma, R.V. Ramanujan, G.P. Tiwari, Instability mechanisms in lamellar microstructures, *Acta Mater.* 48 (2000) 875–889.
- [20] M.E. Keeffe, C.C. Umbach, J.M. Blakely, Surface self-diffusion on Si from the evolution of periodic atomic step arrays, *J. Phys. Chem. Solids* 55 (1994) 965–973.
- [21] S.I. Fujikawa, K.I. Hirano, Y. Fukushima, Diffusion of silicon in aluminum, *Metall. Trans. A* 9 (1978) 1811–1815.
- [22] R.D. Doherty, D.A. Hughes, F.J. Humphreys, J.J. Jonas, D.J. Jensen, M.E. Kassner, W.E. King, T.R. McNelley, H.J. McQueen, A.D. Rollett, Current issues in recrystallization: a review, *Mater. Sci. Eng. A* 238 (1997) 219–274.
- [23] K. Ding, H.C. Liao, Q.M. Jin, Y. Tang, Effect of hot extrusion on mechanical properties and microstructure of near eutectic Al-12.0%Si-0.2%Mg alloy, *Mater. Sci. Eng. A* 527 (2010) 6887–6892.
- [24] Y.N. Wu, H.C. Liao, Y.B. Liu, K.X. Zhou, Dynamic precipitation of Mg₂Si induced by temperature and strain during hot extrusion and its impact on microstructure and mechanical properties of near eutectic Al-Si-Mg-V alloy, *Mater. Sci. Eng. A* 614 (2014) 162–170.
- [25] A.K. Srivastava, V.C. Srivastava, A. Gloter, S.N. Ojha, Microstructural features induced by spray processing and hot extrusion of an Al-18% Si-5% Fe-1.5% Cu alloy, *Acta Mater.* 54 (2006) 1741–1748.
- [26] B. Beausir, J.J. Fundenberger, ATOM — Analysis Tools for Orientation Mapping, Lorraine University, Metz, 2014.
- [27] L.A. Giannuzzi, F.A. Stevie, A review of focused ion beam milling techniques for TEM specimen preparation, *Micron* 30 (1999) 197–204.
- [28] J.J. Fundenberger, A. Morawiec, E. Bouzy, J.S. Lecomte, Polycrystal orientation maps from TEM, *Ultramicroscopy* 96 (2003) 127–137.
- [29] A. Morawiec, J.J. Fundenberger, E. Bouzy, J.S. Lecomte, EP — a program for determination of crystallite orientations from TEM Kikuchi and CBED diffraction patterns, *J. Appl. Crystallogr.* 35 (2002), 287–287.
- [30] S. Dzaszyk, E.J. Payton, F. Friedel, V. Marx, G. Eggeler, On the characterization of recrystallized fraction using electron backscatter diffraction: a direct comparison to local hardness in an IF steel using nanoindentation, *Mater. Sci. Eng. A* 527 (2010) 7854–7864.
- [31] D. Hamilton, R. Seidensticker, Propagation mechanism of germanium dendrites, *J. Appl. Phys.* 31 (1960) 1165–1168.
- [32] X.B. Yang, K. Fujiwara, K. Maeda, J. Nozawa, H. Koizumi, S. Uda, Crystal growth and equilibrium crystal shapes of silicon in the melt, *Prog. Photovolt: Res. Appl.* 22 (2014) 574–580.
- [33] T.H. Courtney, J.C.M. Kampe, Shape instabilities of plate-like structures — II. Analysis, *Acta Metall.* 37 (1989) 1747–1758.